ELSEVIER

Electrical Power and Energy Systems 25 (2003) 443–461

ELECTRICAL POWER & ENERGY SYSTEMS

www.elsevier.com/locate/ijepes

Bifurcations, chaos, and system collapse in a three node power system

Zhujun Jing[a,*], Dashun Xu[b], Yu Chang[c], Luonan Chen[d]

[a]*Institute of Mathematics, Chinese Academy of Sciences, Beijing 100080, People's Republic of China*
[b]*Department of Mathematics and Statistics, Memorical University of Newfoundland, NF, AIC557, Canada*
[c]*Institute of Applied Physics and Computational Mathematics, Beijing 100088, People's Republic of China*
[d]*Department of Electrical Engineering and Electronics, Osaka Sangyo University, 3-1-1 Nakagaito, Daito, Osaka 574-8530, Japan*

Abstract

A model of the three node power system proposed by Rajesh and Padiyar [Electr. Power Energy Syst. 21 (1999) 375] is studied. As the bifurcation parameter P_m (input power to the generator) is changed, the system including the effects of the non-linearity exhibits complex dynamics emerging from static and dynamic bifurcations which link with the system collapse. The analyses for the model exhibit dynamical bifurcations, including three Hopf bifurcations, cyclic fold bifurcations, torus bifurcations and period-doubling bifurcations, and complex dynamical behaviors, including periodic orbits, period-doubling orbits, quasi-periodic orbits, phase-locked phenomena and two chaotic regions between two Hopf bifurcations, i.e. in the 'Hopf window' and intermittency chaos. Moreover, one of the two chaotic regions results from period-doubling bifurcations, and another results from quasi-periodic orbits emerging from a torus bifurcation. Simulations are given to illustrate the various types of dynamic behaviors associated with the power system collapse for the model. In particular, we first shown that the oscillatory transient may play a role in the collapse, and there are different critical points for different dominated state variables. Besides, the hard-limits and increases of the damping factor widen the feasible operating region of the power system, and prevent the torus bifurcation to occur so that some complex dynamical phenomena can be inhibited.

Keywords: Power systems; Chaos; Bifurcations; Hard-limits

1. Introduction

Rajesh and Padiyar investigated dynamical phenomena of the 'two-axis model', the 'one-axis model' and the classical model for power systems in Refs. [16,17]. In the choice of bifurcation parameters, they indicated that the reactive power demand at the load bus as a bifurcation parameter is unrealistic and cannot characterize a wide range of operating conditions. Hence, they took input power to the generator (P_m), the constant real and reactive powers of the motor (P_{ld}, Q_{ld}) and the reference voltage to the AVR (V_{ref}) as the bifurcation parameters, and found out the conditions leading to chaotic behaviors. In particular, they gave a comprehensive study of bifurcations for two-axis model, and also found a torus bifurcation resulting in the emergence of quasi-periodic solutions after a torus bifurcation (TR) induced by a Hopf bifurcation(HB) (corresponding to TR[5] and HB[4] here) for the one-axis model. However, there are still no detail analyses on the one-axis model. In particular, some important behaviors involving phase-locked phenomena and chaos are not given in Ref. [17]. Therefore, Section 4 in this paper aims to investigate the dynamical behaviors emerging from dynamic bifurcations for one-axis model in details. Specifically we first present sustained oscillations and the two chaotic regions via period-doubling and quasi-periodic routes, and show phase-locked phenomena in which the quasi-periodic orbit becomes a complex periodic orbit. Moreover this paper indicates that global dynamic phenomena are drastically affected by the bifurcation parameter P_m, and the state variables dominating system behavior are different at different critical points. In Section 5 of this paper, the effects of the damping factor on the system are considered. When the damping factor is greater than some value, the Hopf bifurcation and the torus bifurcation will be inhibited so that the complex behaviors resulted from the bifurcations can be prevented. However, this role of the damping factor is not as drastic as that of machine damping reported in Ref. [19].

To tackle the problems of voltage stability, the power industry utilizes an emerging control to set the control gains of the excitation voltage profiles and faster voltage

* Corresponding author. Address: Department of Mathematics, Hunan Normal University, Hunan Changsha 410081, People's Republic of China.
E-mail address: jingzj@math03.math.ac.cn (Z. Jing).

0142-0615/03/$ - see front matter © 2003 Elsevier Science Ltd. All rights reserved.
PII: S0142-0615(02)00130-8

responses. However, such excitation control gains also introduce some side-effect problems, and need to be examined so as to better understand the role of excitation voltage controls (especially the excitation hard-limits) in voltage events [11]. Venkatasubramanian made preliminary effort towards developing a formal stability theory for analyzing the various types of hard-limits in Ref. [20]. Recently Ji and Venkatasubramanian [7] studied an interconnected power system modelled by an equivalent single-machine infinite-bus system, and investigated the role of a wind-up type hard-limit present in the excitation control. They showed that at a subcritical Hopf bifurcation where the operating point loses its local stability, the hard-limits could force the transients to converge to a stable limit cycle. Moreover, they illustrated that the limit cycle undergoes further period-doubling cascades that eventually lead to chaos. In Section 6 of this paper, we further introduce a wind-up type hard-limit saturation [8,20] in the excitation control to the one-axis model. We show that the torus bifurcation will be prevented and thereby the complex dynamics resulted from the bifurcation can be eliminated when the saturation model is used.

The rest of the paper is arranged as follows. Section 2 contains a brief description of a power system model. In Section 3, we review some basic bifurcation and chaos theories that are relevant to our studies. The results of bifurcation analyses with some numerical simulation are given in Section 4. The effects of the damping factor on bifurcations are included in Section 5. Section 6 investigates the role of hard-limits in the system and Section 7 is the conclusion of this paper.

2. System model

The power system considered in Ref. [17] is shown in Fig. 1 where we neglect the damper winding on the q-axis and describe the system by the following set of equations: generator model, excitation system for the generator, dynamic load model, and network model.

The dynamics of the generator are described by the rotor mechanical equations and stator equations [14]. Rotor equations for the generator model and the equation for the field winding on d-axis are

$$\dot{\delta} = w_{\mathrm{B}} S_{\mathrm{m}}, \tag{1}$$

$$\dot{S}_{\mathrm{m}} = \frac{-P_{\mathrm{g}} + P_{\mathrm{m}} - dS_{\mathrm{m}}}{2H}, \tag{2}$$

$$\dot{E}'_q = \frac{E_{fd} - E'_q + i_d(x_d - x'_d)}{T'_{d0}}, \tag{3}$$

where d is the damping factor, w_{B} is the system frequency in rad/s, the generator slip S_{m} is defined by $S_{\mathrm{m}} = (w - w_{\mathrm{B}})/w_{\mathrm{B}}$, and the power delivered by the generator P_{g} is expressed as

$$P_{\mathrm{g}} = E'_q i_q + (x'_d - x_q) i_d i_q. \tag{4}$$

Neglected stator transients and the stator resistance, stator equations are given by two algebraic equations as the following:

$$v_q = E'_q + x'_d i_d, \tag{5}$$

$$v_d = -x_q i_q. \tag{6}$$

The equation for the excitation system is given by

$$\dot{E}_{fd} = \frac{-E_{fd} + K_{\mathrm{A}}(V_{\mathrm{ref}} - V_t)}{T_{\mathrm{A}}}, \tag{7}$$

where V_{ref} is the reference voltage to the AVR.

The load model includes a dynamic induction motor based on a model defined by Walve [21] and a constant PQ load in parallel. The induction motor model specifies the real and reactive power demands P and Q of the motor in terms of load voltage V and frequency ω. The combined model for the motor and the PQ load is

$$P = P_{ld} + P_0 + p_1 \dot{\delta}_{\mathrm{L}} + p_2 \dot{V}_{\mathrm{L}} + p_3 V_{\mathrm{L}}, \tag{8}$$

$$Q = Q_{ld} + Q_0 + q_1 \dot{\delta}_{\mathrm{L}} + q_2 V_{\mathrm{L}} + q_3 V_{\mathrm{L}}^2, \tag{9}$$

where P_{ld} and Q_{ld} are the constant real and reactive powers of the motor, and P_0 and Q_0 represent the PQ load.

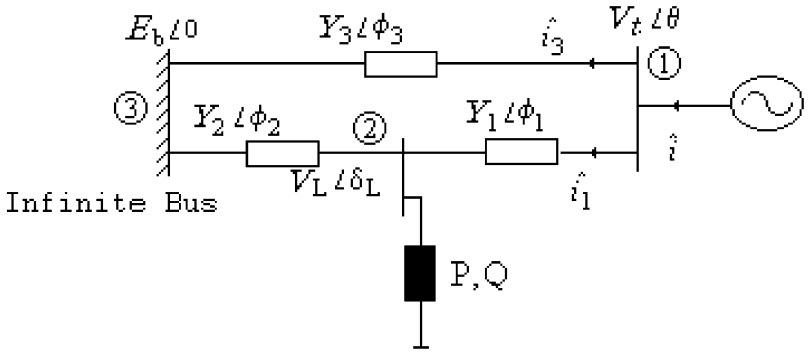

Fig. 1. A three-node power system model.

The network model in the D–Q reference frame is written as

$$i_q \cos(\phi) + i_d \sin(\phi) = Yv_q - a, \tag{10}$$

$$i_d \cos(\phi) - i_q \sin(\phi) = Yv_d - b, \tag{11}$$

where

$$a = V_L Y_1 \cos(\delta_L - \delta - \phi + \phi_1) + E_b Y_3 \cos(\delta + \phi - \phi_3),$$

$$b = V_L Y_1 \sin(\delta_L - \delta - \phi + \phi_1) - E_b Y_3 \sin(\delta + \phi - \phi_3).$$

The real and reactive powers supplied to the load by the network are

$$P = -V_L^2 Y_1 \cos(\phi_1) - V_L^2 Y_2 \cos(\phi_2) + V_L V_t Y_1 \cos(r_1) + E_b V_L Y_2 \cos(r_2), \tag{12}$$

$$Q = V_L^2 Y_1 \sin(\phi_1) + V_L^2 Y_2 \sin(\phi_2) + V_L V_t Y_1 \sin(r_1) + E_b V_L Y_2 \sin(r_2), \tag{13}$$

where

$$\theta = \delta + \arctan\left(\frac{v_d}{v_q}\right), \quad r_1 = \delta_L - \theta - \phi_1, \quad r_2 = \delta_L - \phi_2,$$

$$V_t = \sqrt{v_d^2 + v_q^2}.$$

Substituting from Eqs. (10)–(13) in Eqs. (1)–(3) and Eqs. (8) and (9), and rearranging Eqs. (8) and (9) so that $\dot{\delta}_L$ and $\dot{V}_L$ appear on the left-hand side, we obtain the following power system model.

$$\begin{cases} \dot{\delta} = w_B S_m \\ \dot{S}_m = \dfrac{-P_g + P_m - dS_m}{2H} \\ \dot{E}'_q = \dfrac{E_{fd} - E'_q + i_d(x_d - x'_d)}{T'_{d0}} \\ \dot{E}_{fd} = \dfrac{-E_{fd} + K_A(V_{ref} - V_t)}{T_A} \\ \dot{\delta}_L = (Q - Q_{ld} - Q_0 - q_2 V_L - Q_3 V_L^2)/q_1 \\ \dot{V}_L = (P - P_{ld} - P_0 - p_1 \dot{\delta}_L - p_3 V_L)/p_2 \end{cases}. \tag{14}$$

All of the parameters in Eq. (14) will be fixed except P_m, i.e. P_m will be taken as the bifurcation parameter. We follow Ref. [17] by using the following parameter values.

$Y_1 = 4.9752$, $Y_2 = 1.6584$, $Y_3 = 1.1056$, $\phi_1 = \phi_2 = \phi_3 = -1.4711$, $E_b = 1.0$, $x_d = 1.79$, $x_q = 1.71$, $T'_{d0} = 4.3$, $T'_{q0} = 0.85$, $x'_d = 0.169$, $x'_q = 0.23$, $H = 2.894$, $w_b = 377$, $d = 0.05$, $E_m = 1.0P_0 = 0.4$, $Q_0 = 0.8$, $p_1 = 0.24$, $q_1 = -0.02$, $p_2 = 1.7$, $q_2 = -1.866$, $p_3 = 0.2$, $q_3 = 1.4$, $K_A = 200$, $T_A = 0.05$.

3. Review of bifurcation and chaos

In this section, we give a brief review of bifurcations and chaos in Refs. [6,12,22] which are examined in a more intensive manner in this paper. By definition, bifurcations occur at those parameter values where there is a change in the system's qualitative properties.

The power system model of Eq. (14) can be written as an autonomous differential equation of the form with μ as a bifurcation parameter

$$\dot{x} = f(x, \mu), \quad x \in \mathbf{R}^6, \quad \mu \in \mathbf{R}, \quad f \in C^r, \quad r \geq 2, \tag{15}$$

where generally the state vector x may consist of generator angle, generator angular velocity, load voltage magnitude, etc. the parameter μ may be real, reactive power or input power to the generator, etc.

At a fixed point (a equilibrium point or a steady-state solution) $x(\mu_0)$, since the right-hand term of Eq. (15) becomes zero, its stability is dominated by the eigenvalues of the Jacobian $J = \partial f/\partial x$ evaluated at $x(\mu_0)$. Define the eigenvalues of J to be $\lambda_i(\mu_0)$, $i = 1, 2, \ldots, 6$. $x(\mu_0)$ is hyperbolic if $Re[\lambda_i(\mu_0)] \neq 0$, for all $i = 1, 2, \ldots, 6$; $x(\mu_0)$ is non-hyperbolic if there exists j such that $Re[\lambda_j(\mu_0)] = 0$.

3.1. Saddle-node bifurcation (SNB)

At a SNB point, two equilibrium points, generally one stable and one unstable, coalesce and become a saddle-node point, and then disappear as the parameter passes through the bifurcation value. For the SNB, J has a simple zero eigenvalue with the remaining eigenvalues having non-zero real parts. Therefore, the necessary conditions for SNB are given by

$$f(x_0, \mu_0) = 0, \qquad \det J(x_0, \mu_0) = 0.$$

Not all points satisfying these necessary conditions are SNB points (the points satisfying these conditions can be transcritical or pitchfork bifurcation). To illustrate the nature of sufficient conditions we consider a scalar system or reduce the system to one-dimensional system by the center manifold theorem. For such a system $f(x, \mu)$, the sufficient conditions for SNB are:

$$f(x_0, \mu_0) = 0, \qquad \left.\frac{\partial f}{\partial x}\right|_{(x_0,\mu_0)} = 0, \qquad \left.\frac{\partial f}{\partial \mu}\right|_{(x_0,\mu_0)} \neq 0,$$

$$\left.\frac{\partial^2 f}{\partial x^2}\right|_{(x_0,\mu_0)} \neq 0.$$

SNB is considered as a main reason for dynamic instability of the system (15) and is associated with voltage collapse problems in power systems [3,4,9].

3.2. Hopf bifurcation

Hopf bifurcation (HB) does not yield any changes in the number of equilibrium points. This type of bifurcations are

characterized by a complex conjugate pair of eigenvalues for $x(\mu_0)$ lying on the imaginary axis of the complex plane, and result in the birth or death of a stable or unstable limit cycle.

The Hopf bifurcation theorem [6] states that under certain conditions a branch of periodic solutions splits off from a equilibrium when some parameters change. The crucial hypotheses made in the theorem for Eq. (15) are the Jacobian matrix $A(\mu) = D_x f(x_0(\mu), \mu)$ has a pair of complex conjugate eigenvalues, $\alpha(\mu) \pm i\beta(\mu)$ and for some value $\mu = \mu_0$

$$\alpha(\mu_0) = 0, \qquad \beta(\mu_0) > 0,$$

and

$$\alpha'_\mu(\mu_0) \neq 0,$$

and the remaining eigenvalues of $A(\mu_0)$ have non-zero real parts. Next we summarize the conditions for deciding Hopf bifurcation of the six-order system of Eq. (14) according to Ref. [18].

Theorem: suppose that the differential equation (15) has an equilibrium point $x = x_0(\mu)$, the characteristic equation of the Jacobian matrix $A(\mu) = D_x f(x_0(\mu), \mu)$ is

$$P(\lambda) = \lambda^6 + c_1\lambda^5 + c_2\lambda^4 + c_3\lambda^3 + c_4\lambda^2 + c_5\lambda + c_6 = 0,$$

if the following conditions are satisfied:

(i) there exists $\mu = \mu_0$ such that $c_i(\mu_0) > 0$ for all $i = 1, 2, \ldots, 6$, and

$$\begin{aligned} H_5(\mu_0) = &-c_3^2c_4c_5 + c_2c_3c_5^2 - c_5^3 + c_3^3c_6 - c_1^3c_6^2 \\ &+ c_1^2(-c_4^2c_5 + c_3c_4c_6 + 2c_2c_5c_6) \\ &- c_1(c_2^2c_5^2 + c_2c_3(c_3c_6 - c_4c_5) + c_5(3c_3c_6 - 2c_4c_5) = 0, \end{aligned}$$

(ii)

$$\begin{aligned} H_4(\mu_0) = &-c_3^2c_4 + c_2c_3c_5 - c_5^2 + c_1^2(c_2c_6 - c_4^2) + c_1(c_2c_3c_4 \\ &- c_2^2c_5 + 2c_4c_5 - c_3c_6) \neq 0, \end{aligned}$$

and

$$H_3(\mu_0) = -c_3^2 - c_1^2c_4 + c_1(c_2c_3 + c_5) \neq 0,$$

(iii)

$$\left.\frac{dH_5(\mu)}{d\mu}\right|_{\mu=\mu_0} \neq 0,$$

then there is a Hopf bifurcation. The equilibrium $x(\mu_0)$ may bifurcate into 'small amplitude' periodic solutions as the value μ passes through μ_0. In other words, the periodic solution will emerge when $\mu < \mu_0$ or $\mu > \mu_0$ is sufficiently close to μ_0.

Remark 1. The characteristic equation has a pair of purely imaginary real roots if the condition (i) of the theorem is satisfied. The conditions (ii) and (iii) are referred to as the transverse condition of Hopf bifurcation theorem [6].

Remark 2. A Hopf bifurcation is said to be subcritical or supercritical if the periodic solutions are unstable or stable. In particular, a subcritical Hopf bifurcation may induce voltage collapse phenomena [1,3,19].

3.3. Cyclic fold, period-doubling bifurcation, torus bifurcation, phase-locked phenomena

The stability of the branch of periodic solutions created from Hopf bifurcations can be determined by Floquet multipliers.

Letting the periodic solution of Eq. (15) at $\mu = \mu_0$ be $x(t, \mu_0)$ and have the minimal period T, then the local behavior near $x(t, \mu_0)$ is determined by linearizing Eq. (15) along $x(t, \mu_0)$. The linearized equation is

$$\dot{y} = D_x f(x(t, \mu_0), \mu_0)y.$$

It is a six-dimensional linear system and has six linearly independent solutions y_i, where $i = 1, 2, \ldots, 6$. These solutions can be expressed in the form of an 6×6 matrix called a fundamental matrix solution as

$$Y(t) = [y_1(t), y_2(t), \ldots, y_6(t)].$$

Obviously, Y satisfies the matrix equation

$$\dot{Y} = D_x f(x(t, \mu_0), \mu_0)Y.$$

When $\Phi(t)$ satisfies the above matrix equation and the initial condition

$$\Phi(0) = I,$$

where I is the 6×6 identity matrix, $\Phi(T)$ is called the monodromy matrix, and the eigenvalues of the monodromy matrix are called the Floquet or characteristic multipliers [12]. Ref. [15] provides the detail procedure to calculate the Floquet multipliers of a periodic solution.

The monodromy matrix has six Floquet multipliers. One of them associated with a periodic solution $x(t, \mu)$ is always unity and the other five multipliers $\eta_i(\mu)$, $i = 1, 2, \ldots, 5$, determine the stability of $x(t, \mu)$ by the rule: $x(t, \mu)$ is stable if $|\eta_i(\mu)| < 1$ for all $i = 1, 2, \ldots, 5$; $x(t, \mu)$ is unstable if $|\eta_i(\mu)| > 1$ for some i.

When we change the parameter μ, the multipliers $\eta_i(\mu)$ also vary because the multipliers are the functions of the parameter, therefore depending on the parameter. Generically there exist three different ways in which multipliers cross the unit circle [12].

(i) Only one real multiplier crosses the unit circle along the positive real axis, i.e. there exists $\eta(\mu_c) = 1$.
(ii) Only one real multiplier crosses the unit circle along the negative real axis, i.e. there exists $\eta(\mu_c) = -1$.
(iii) A pair of complex conjugate multipliers crosses the unit circle with a non-zero imaginary part, i.e. there exists $\mathrm{Im}(\eta(\mu_c) \neq 0$.

In the first case, a stable periodic solutions and an unstable periodic solutions, coalesce and obliterate each other at the bifurcation point μ_c which is called cyclic fold bifurcation just like saddle-node bifurcation for fixed points in the Poincaré map. When the function f satisfies some symmetry or other regularity properties, pitchfork or transcritical bifurcation may occur [6,22]. The flip bifurcation of the double period bifurcation occurs in the second case, where a branch of period-doubled solutions is created or destroyed at the critical value μ_c. If the bifurcation is supercritical, a branch of stable period-doubled solutions emerges, and the original branch of stable periodic solutions continues as a branch of unstable periodic solutions at the post-bifurcation. On the other hand, if the bifurcation is subcritical, a branch of unstable period-doubled solutions is destroyed, and the original branch of stable periodic solutions continues as a branch of unstable periodic solutions at the post-bifurcation. In the third case, the bifurcation generates a torus, which is called secondary Hopf bifurcation, Hopf bifurcation of the periodic orbit or torus bifurcation.

After the bifurcation from a periodic orbit (with frequency $\omega_1(\mu_0)$) to a torus, there are two frequencies: $\omega_1(\mu_0)$ and $\omega_2(\mu_0)$. The related flow on the torus is called a quasi-periodic solution if ω_1 and ω_2 are incommensurate (i.e. ω_1/ω_2 is irrational). For some μ, ω_1 and ω_2 are commensurate, then the trajectory on the torus is closed and periodic, which is called phase-locked or frequency-locked phenomenon. Higher dimensional tori have more frequencies. Rotation number and Arnold tongue well describe the nature of the phenomenon [6,12,22].

3.4. Routes to chaos

Chaotic solutions are identified with non-periodicity and sensitive dependence on initial conditions. Hence, chaos is complicated geometrical objects that possess fractal dimensions. We denote the flow generated by Eq. (15) by $\phi(x,t)$ and assume that it exists for all $t > 0$. And assume that $\Lambda \subset \mathbb{R}^6$ is a compact set invariant under $\phi(x,t)$, i.e. $\phi(\Lambda,t) \subset \Lambda$ for all $t > 0$. Then the generally acceptable definitions for the sensitive dependence and chaos are given in Ref. [6].

Definition 1. The flow $\phi(x,t)$ is said to have sensitive dependence on initial conditions on Λ if there exists $\varepsilon > 0$ such that, for any $x \in \Lambda$ and any neighborhood U of x, there exists $y \in U$ and $t > 0$ such that $|\phi(x,t) - \phi(y,t)| > \varepsilon$.

Roughly speaking, Definition 1 implies that for any point $x \in \Lambda$ there is (at least) one point arbitrarily close to Λ that diverges from x.

Definition 2. Λ is said to be chaotic if

(i) $\phi(x,t)$ has sensitive dependence on initial conditions on Λ.
(ii) $\phi(x,t)$ is topologically transitive on Λ.
(iii) The periodic orbits of $\phi(x,t)$ are dense in Λ.

Remark. In Ref. [22], the (iii) is not explicitly included in the definition of a chaotic invariant set because a closed invariant set Λ is topologically transitive if a point $y \in \Lambda$ exists such that its orbit is dense in Λ.

Definition 3. Suppose $A \subset \mathbb{R}^6$ is an attractor, then A is called a strange attractor if it is chaos.

Presently, there are many fairly well understood transitions or routes to chaos. In this paper, we only introduce three routes to chaos: periodic doubling bifurcation, intermittency and torus breakdown, which are observed in the dynamical simulation of power systems.

Recall that before a supercritical period-doubling bifurcation, there exists a branch of stable periodic solutions, and after the bifurcation, there exists a branch of stable period-two solutions (period-doubled solutions). If the branch of period two solutions repeat the same bifurcation as the parameter is varied, a branch of period four solutions is created. And so fourth, one can expect a branch of period 2^n solution, and finally a branch of chaotic attractors appears. This is called a period-doubling cascade to chaos. There are many researches about it in power systems [2,3,10,13].

Intermittency is also a route to chaos observed frequently in physical experiments. We describe the main features of the route. For values of a parameter μ less than a critical value μ_c, the system oscillates in a regular mode, and there exists a stable periodic solution for the system. As μ changes and is slightly more than a threshold value μ_c, the oscillations seems to be regular and closely similar to the behaviors for $\mu < \mu_c$, but they are occasionally interrupted by turbulent bursts of aperiodic oscillations at irregular intervals. With increasing μ, the time intervals (the time regular oscillation) between two consecutive bursts become smaller and smaller and more and more difficult to be distinguished. As μ is increased further, the periodic oscillations disappear and are completely replaced with chaotic response.

Chaos also can appear following a torus characterized by two oscillatory modes with incommensurate frequencies. As the parameter μ is varied, if a branch of stable periodic solution undergoes a supercritical secondary Hopf bifurcation, a branch of two period quasi-periodic solution with two incommensurate frequencies appears. With increasing μ, a rich variety of bifurcations of the torus can take place. One of those post-bifurcation states is a chaotic attractor. As the parameter is varied, the two-torus is deformed, destroyed, and chaos emerges at last. In this scenario, the closed curve of the two quasi-periodic solutions in the Poincare section deforms, wrinkles, and becomes fractal, and finally breaks down. Since the transition to chaos from torus fulfills through the destruction of the closed curve, this transition is often described as chaos via torus breakdown.

3.5. Identifying chaos

To decide whether an oscillation is chaotic, there are several numerical indices such as fractal dimensions, Fourier spectra, and Lyapunov exponents. Just like what we did in Section 4, we can also distinguish among fixed points, periodic oscillations, quasi-periodic solutions and chaotic solutions by using Lyapunov exponents. Chaotic attractor can be seen as the result of an infinite number of stretchings in one or more directions and contractions in another or some other directions, combined with foldings, where Lyapunov exponents just measure these stretchings and contractions.

The linearization of Eq. (15) is the variational equation

$$\dot{y} = f_x(x, \mu)y,$$

where the Jacobian f_x is evaluated along the particular trajectory $x(t, x_0)$. For any initial vector $y(0)$, the solution $y(t)$ can be expressed

$$y(t) = \Phi(t)y(0).$$

Here the fundamental solution matrix $\Phi(t)$ comes from

$$\dot{\Phi} = f_x(x(t, x_0), \mu)\Phi, \qquad \Phi(0) = I.$$

Let the eigenvalues of $\Phi(t)$ be $\lambda_i(t)$, $i = 1, 2, \ldots, 6$, then these eigenvalues represent the stretching of the principal axes. Now we give the definition of Lyapunov exponents:

$$L_k = \lim_{t\to\infty} \frac{1}{t}\ln(\lambda_k(t)), \qquad k = 1, 2, \ldots, 6.$$

From this definition, we can see that L_i represents the average rate of stretching or contraction of the ith direction in the phase space $\mathbb{R}^6$ along the solution $x(t, x_0)$. That is to say, the trajectory will dispel others nearing it in a particular direction along it if a Lyapunov exponent is positive, otherwise, the trajectory will attract others nearing it in a particular direction along it. Hence for dissipative systems, the sum of all Lyapunov exponents must be negative, $\sum_i L_i < 0$.

For a fixed point, when all Lyapunov exponents are negative, the point is a stable fixed point. For a limit cycle of an autonomous system, one of the Lyapunov exponents is always zero, and for a stable periodic orbit, all Lyapunov exponents except one zero eigenvalue are negative. For a m-torus, there are m Lyapunov exponents equal to zero. When all other Lyapunov exponents are negative, the torus is stable. In dissipative systems, chaos are characterized by one or more positive Lyapunov exponents, which correspond to the nature of sensitivity to initial conditions. However, a positive Lyapunov exponents is a necessary but not sufficient condition for chaos, it is still the standard by which we confirm chaotic behaviors in numerical simulations. For a detailed discussion, see Ref. [12].

4. Bifurcation analysis and chaos

In this section, we analyze the stability and bifurcation for Eq. (14) where P_m is taken as a bifurcation parameter. All the results are obtained by detailed numerical simulations, and preliminary analyses are based on the mathematical theories and methods of Section 3.

First of all, the bifurcation diagram is given in Fig. 2 by using AUTO97 [5]. There are twelve types of bifurcations, which are listed in Table 1.

From Fig. 2, we show that the equilibrium point $x_2(P_m)$ undergoes four bifurcations labelled as HB^1, HB^2, HB^3 and SNB^4. The equilibrium point $x_2(P_m)$ is stable for $0 < P_m < P_m^4 = 0.608664$, but as P_m is increased, the equilibrium $x_2(P_m)$ loses its stability at $P_m = P_m^4$ through HB^4. With a further increase in P_m, the $x_2(P_m)$ gains stability through HB^1 at $P_m = P_m^1 = 1.155867$. It remains stable until $P_m = P_m^2 = 1.191285$, where stability is lost through HB^2. Further the SNB^3 does not influence the stability of $x_2(P_m)$. The movement of six eigenvalues of the Jacobian matrix at x_2 is shown in Fig. 3 by numerical simulation as the parameter P_m varies.

At $P_m = P_m^4$, a supercritical Hopf bifurcation HB^4 occurs. The Jacobian matrix at the equilibrium x_2 has a pair of pure imaginary eigenvalues and four negative real part eigenvalues: $\{\pm 33.6677j, -32.19, -7.7426, -1 \pm 6.8525j\}$. Fig. 3(a) shows the pair of conjugate complex eigenvalues transversely crosses the ωj axis at E and e from the left to the right half plane while $P_m = P_m^4$, E and e in Fig. 3(b) and (c) show the four eigenvalues with negative real parts, so a supercritical Hopf bifurcation occurs at $P_m = P_m^4$, and the equilibrium x_2 becomes unstable for $P_m > P_m^4$. Due to the pair of pure imaginary eigenvalues, $\pm\omega_0 j = \pm 33.6677j$, there is a stable periodic solution with the period approximately equal to $2\pi/\omega_0$ for P_m slightly more than P_m^4 by the Hopf theorem. We check that for $P_m = 0.6099$ there exists a stable periodic solution with a period of $T = 2\pi/\omega_0 \approx 0.18$ s by numerical simulation. Hence, at the critical point HB^4, system behavior is dominated by δ and S_m.

At the critical points HB^1 and HB^2, the eigenvalues of the Jacobian at x_2 are $\{\pm 31.2075j, -20.809, -13.085, -0.12 \pm 7.543j\}$ and $\{-0.3757 \pm 30.88j, -19.73, -13.95, \pm 7.57j\}$, respectively. From Fig. 3(a), we can see that the curves re-cross the ωj axis at points A and a ($\pm\omega_0^1 j = \pm 31.2075j$ corresponding to δ and S_m) leading to the subcritical Hopf bifurcation HB^1 at $P_m = P_m^1$, and other real parts of the eigenvalues are negative (see points A and a in Fig. 3(b) and (c)), so x_2 remains stable until $P_m = P_m^2 = 1.191285$. At $P_m = P_m^2$, another pair of complex eigenvalues crosses the ωj axis transversely ($\pm\omega_0^2 j = \pm 7.57321j$ corresponding to δ_L and V_L) from the left to the right half plane, which are shown by points B and b in Fig. 3(b), so a subcritical Hopf bifurcation HB^2 occurs again, and x_2 re-losses stability due to it and remains unstable until $P_m = P_m^3$. At P_m^1 and P_m^2, HB^1 and HB^2 are both subcritical. There

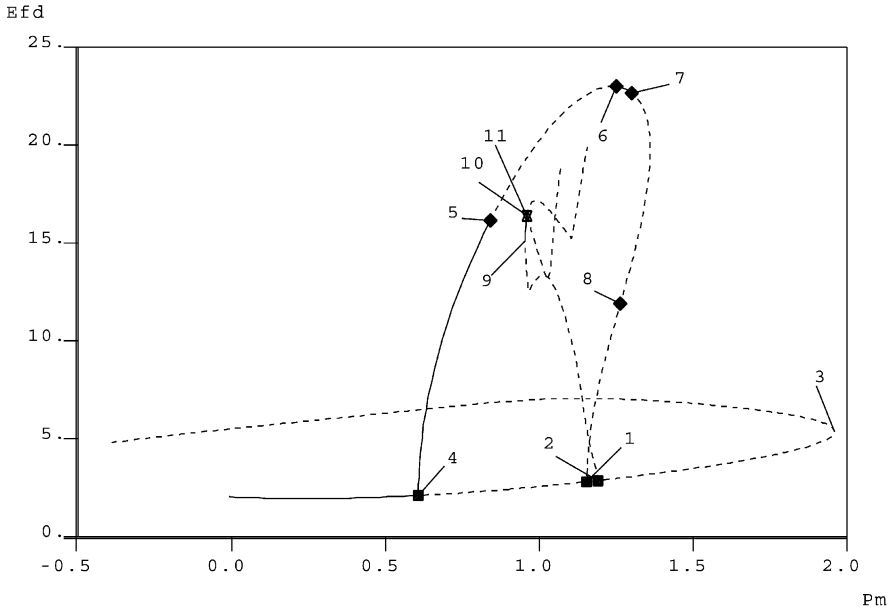

Fig. 2. Bifurcation diagram of $E_{fd} - P_m$, the solid and the dotted line represent the stable and the unstable stationary points (or periodic solutions), respectively.

are unstable oscillations with periods approximately equal to $2\pi/\omega_0^1$ and $2\pi/\omega_0^2$ for P_m slightly more than P_m^1 and P_m slightly less than P_m^2, respectively. But the periods of the unstable oscillations near them are not checked in this paper. At the critical points HB^1 and HB^2, system behavior is dominated by δ, S_m and δ_L, V_L, respectively.

At $P_m^3 = 1.960761$, a saddle-node bifurcation SNB^3 occurs, at which the Jacobian has a simple zero eigenvalue, a real positive eigenvalue and two pairs of complex eigenvalues with negative real parts: $\{-11.044 \pm 21.9116, -14.2932 \pm 14.7414, 8.38915, 0\}$ (see points C and c in Fig. 3). The system has no operating point for $P_m > P_m^3 = 1.960761$.

Fig. 2 also shows the branches of the periodic solutions emerging from HB^4, HB^1 and HB^2. As HB^4 is supercritical, a family of stable periodic orbits emanates from HB^4, and the six multipliers of the stable periodic orbits lie inside the unit circle. As P_m increases, the stable orbits lose their stabilities due to a torus bifurcation TR^5 at $P_m^5 = 0.840966$, the corresponding six multipliers are $\{1, 0.0005, 0.190515 \pm 0.981684j, 0.23067 \pm 0.156288j\}$, where the pair of complex conjugate multipliers $0.190515 \pm 0.981684j$ passes across the unit circle from the inside to the outside the unit circle with an increase in P_m, so that a torus bifurcation occurs at $P_m = P_m^5$ and the periodic oscillation loses its stability for $P_m > P_m^5$. With further increases in P_m, the periodic orbit gains it back at TR^6 at $P_m = 1.251128$, and it remains stable until TR^7. At TR^6, a pair of complex conjugate multipliers $-0.543321 \pm 0.83952234j$ goes to the inside the unit circle, and other multipliers lie inside the unit circle. The periodic oscillation loses its stability through TR^7 at $P_m^7 = 1.30209$. From P_m^7, it has not regained its stability although it goes through TR^8. The branch emerging from HB^1 is the same as that from HB^4.

On the branch emerging from HB^2, unstable periodic oscillations emerge from HB^2 at $P_m^2 = 1.191285$ where one of the multipliers lie outside the unit circle. As P_m decreases, the multiplier enters the unit circle at $P_m^9 = 0.954709$ from the positive side of the real axis, so that the periodic branch turns to the right and gains its stability through circle fold bifurcation CFB^9. However, with increasing P_m, one of the multiplier crosses the unit circle at -1 for $P_m^{10} = 0.960252$, which results in the period-doubling bifurcation PDB^{10}. And then the periodic solution undergoes a cascade of period-doubling bifurcations at PDB^{11} and PDB^{12}.

Next, we further analyze the complex dynamical properties of the system emerging from HB^4 and HB^2 by using the detailed numerical analysis based on the computations of the largest Lyapunov exponent, the projections and the time domain plot of the trajectories.

Table 1
All bifurcation points in Fig. 2 and their P_m values for $d = 0.05$

	P_m		P_m
HB^1	1.155867	TR^7	1.30209
HB^2	1.191285	TR^8	1.264726
SNB^3	1.960761	CFB^9	0.954709
HB^4	0.608664	PDB^{10}	0.960252
TR^5	0.840966	PDB^{11}	0.962034
TR^6	1.251128	PDB^{12}	0.962452

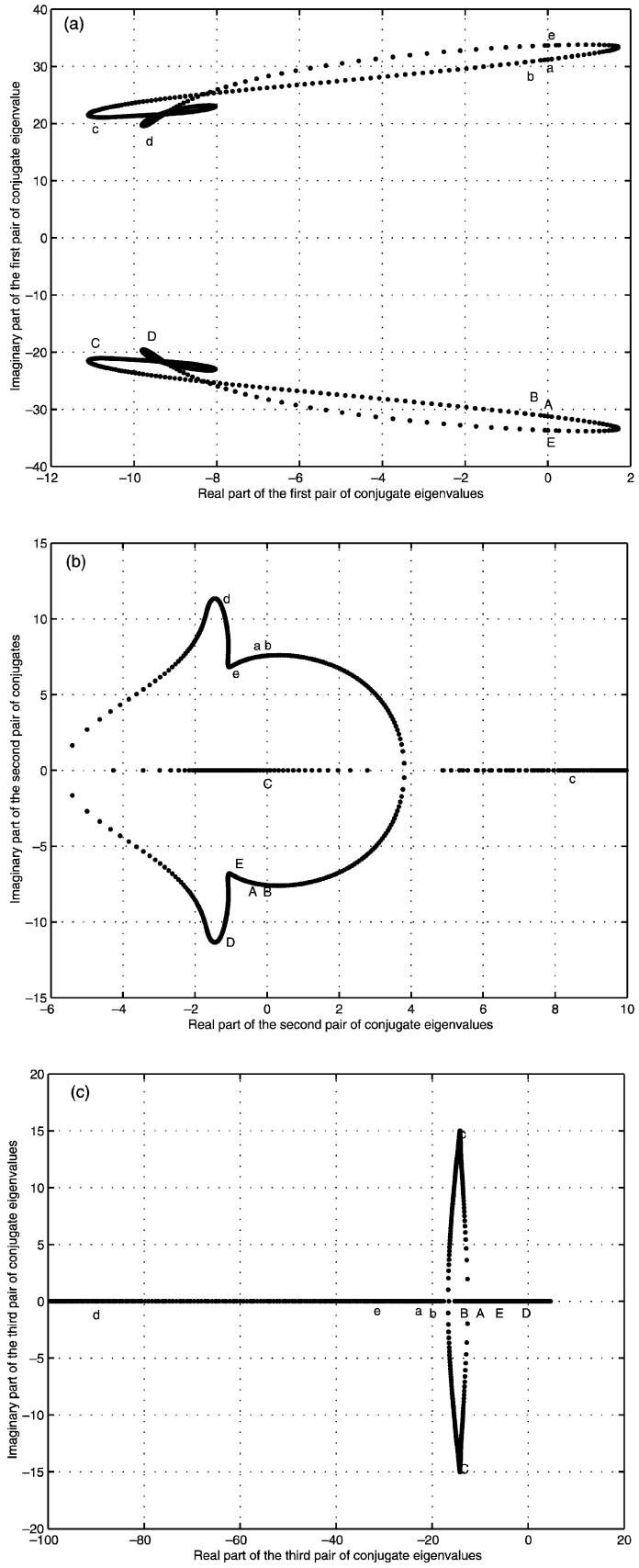

Fig. 3. As P_m increases, the eigenvalues cross the points $E \rightarrow A \rightarrow B \rightarrow C \rightarrow D$ or $e \rightarrow a \rightarrow b \rightarrow c \rightarrow d$. (a)–(c) show the movements of three pairs of conjugate eigenvalues.

4.1. Dynamics emerging from HB[4]

On the continuation of HB[4], we first find a family of stable periodic solutions which are shown in Fig. 4. The periodic solution encounters the torus bifurcation TR[5] at $P_m^5 = 0.840966$, and the bifurcation results in the emergence of quasi-periodic solution so that the periodic branch loses its stability. For $P_m^5 < P_m \leq 1.043$, the trajectories starting from the neighborhood of the stationary point tend to a quasi-periodic oscillation. Fig. 5 shows that the toroidal attractor expands in the sense of the slowly increasing amplitude of the oscillations while P_m is built up in the interval. The approximate frequencies of the oscillations in Fig. 5 roughly consist of $\omega_1 = 33.39$ and $\omega_2 = 7.13$ for $P_m = 0.851$. We also give the approximate frequencies of the oscillations for quasi-periodic trajectory are $\omega_1 = 33.151$ and $\omega_2 = 7.196$ for $P_m = 0.901$, $\omega_1 = 32.17069$ and $\omega_2 = 7.40735$ for $P_m = 1.043$, and drew the projections of quasi-periodic trajectory for $P_m = 0.901$ and 1.043, which have analogy to Fig. 5, we omitted these. Those frequencies, respectively, come from the imaginary parts of the complex eigenvalues at the corresponding P_m values.

When we carefully check the variation of the quasi-periodic oscillation further, it is of interest to note that phase-locked phenomena suddenly emerge. When P_m is in the little right neighborhood of 1.043, the toroidal attractor has already been deformed. As a result of the deformation, the unlocking phenomena suddenly occur when P_m is slightly more than 1.0431, and the toroidal attractor completely changes into a complex periodic orbit. The projections of the periodic orbits are shown in Fig. 6 for $P_m = 1.0432$ and $P_m = 1.04547$. The periodic orbits last until P_m is approximately equal to 1.09.

When $P_m = 1.09706$, we find a chaotic attractor, whose projection of the chaotic attractor is shown in Fig. 7, and the solution is interrupted by bursts. By carefully checking the bursts of the solutions, it has been found that the time between two bursts are almost the same, and the largest Lyapunov exponent (L_1) of the trajectory in Fig. 7 for $P_m = 1.09706$ is positive and approximate to 0.004. As P_m continues to increase slowly, the turbulent bursts occur more and more frequently and the largest Lyapunov exponent is 0.0022 for $P_m = 1.105$, we drew the figure, but omitted it here.

When P_m reaches up to 1.117, the largest Lyapunov exponent of the strange attractor is 0.1437. With a further increase in P_m, where the largest Lyapunov exponent of the chaotic attractors is 0.1447. The approximate frequencies of the chaotic oscillations are related to the imaginary parts of the complex eigenvalues of the Jacobian matrix linearized at the corresponding fixed points.

When P_m continuously increases, we find a group of trajectories which are shown in Figs. 7 and 8. Carefully comparing the projections of these trajectories, a cascade of period-doubling bifurcations can be identified. Fig. 7 shows a period orbit with a long period, while Fig. 8 shows the doubled orbits which finally merge in to a chaotic orbit at $P_m = 1.12923$. We show that there is an 'burst' in chaotic behavior which has an 'intermittency' mechanism. We drew the projectory and the corresponding behaviors of E_{fd} and V_L, but omitted it. The largest Lyapunov exponent is 0.146 for $P_m = 1.12923$.

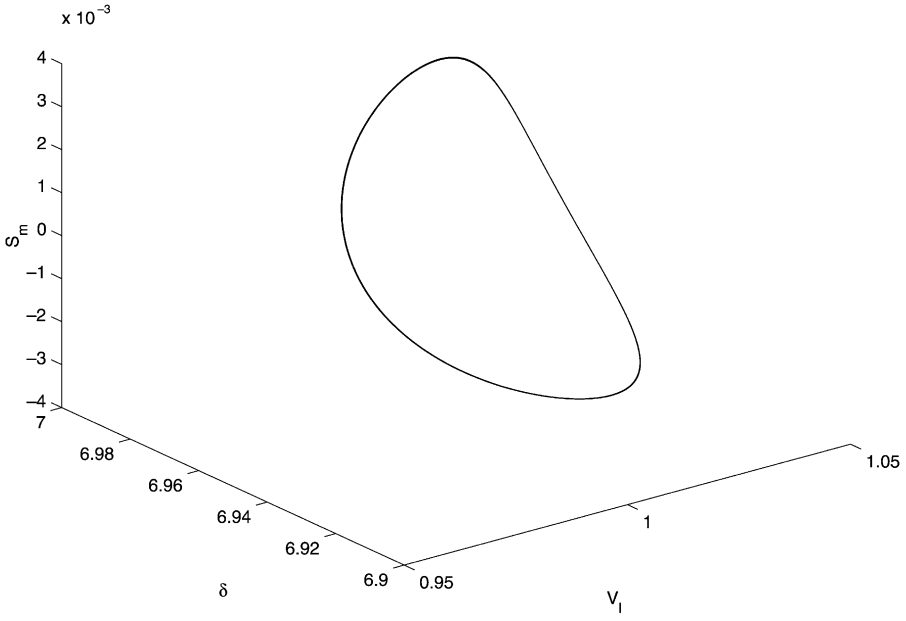

Fig. 4. The projections of the periodic trajectory for $P_m = 0.74603072$.

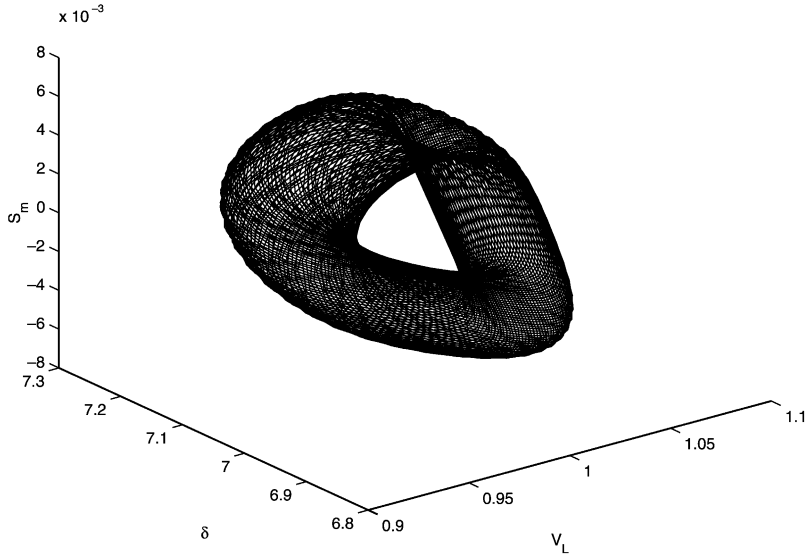

Fig. 5. The projection of quasi-periodic trajectory for $P_m = 0.851$.

The chaotic oscillating modes last until P_m is approximately equal to 1.135. Fig. 9 exemplifies the mode. From Fig. 9, we can see the trajectory is burst frequently by turbulent contractions. The behavior of the system becomes to be quite complex for $P_m = 1.1295$ and 1.135. As P_m grows up further, the turbulent contractions occurs more and more frequently. At last, the trajectory diverges for the variables δ and δ_L.

4.2. Dynamics emerging from HB^2

As HB^2 is subcritical, the periodic branch from HB^2 gains the stability through CFB[9]. With increases of P_m, the stable periodic solution encounters PDB[10], and bifurcates to a period-two branch which bifurcates to a new period four branch when it is subjected to PDB[11]. With this pattern, the periodic branch finally reaches chaos at $P_m = 0.963$. Fig. 10(a)–(d) show the projection of a period-one solution and its sample time simulations at $P_m = 0.9554$, and the projection of period-two for $P_m = 0.961$, four for $P_m = 0.9627$ and eight for $P_m = 0.9623$, and their sample time simulations are, respectively, found, we only give the plot of period-two for $P_m = 0.961$ in Fig. 11. Fig. 12 shows the projection of the chaotic trajectory whose largest Lyapunov exponent is 0.3465 which verifies the chaotic feature at $P_m = 0.965$. Fig. 12 shows the sample time simulation. Chaos resulted from cascades of period-doubling bifurcations is observed in the region around $P_m \in$

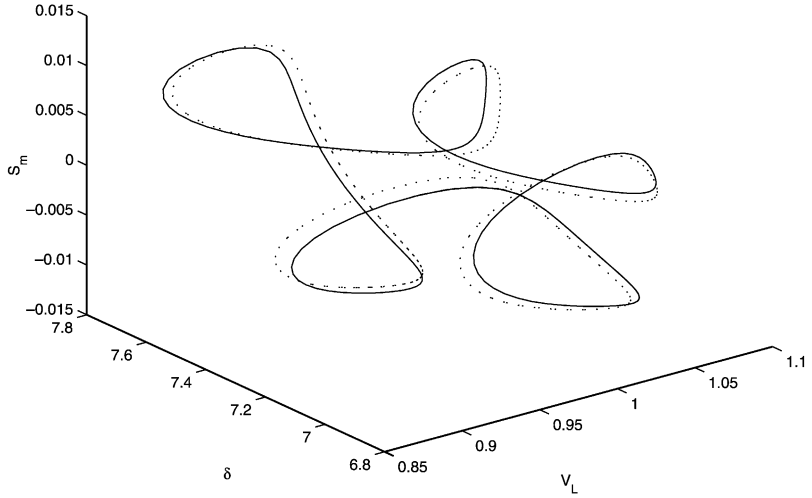

Fig. 6. The dot line represents the projection of the periodic orbit for $P_m = 1.0432$, and the solid line represents that for $P_m = 1.04547$.

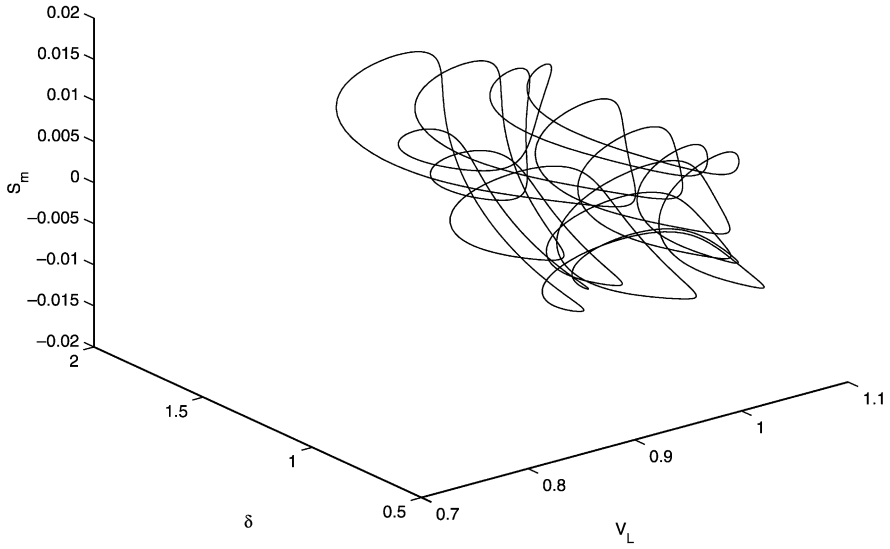

Fig. 7. The projection of the periodic trajectory for $P_m = 1.128$.

[0.963, 0.965], and when $P_m > 0.966$, the chaotic trajectory becomes a quasi-periodic solution.

5. The effects of damping factor on bifurcations and dynamics

In this section, we investigate the loci of bifurcation points for system (14) when both P_m and d are varied. From Eq. (14), we know that the damping factor d does not affect the locations of equilibrium points, which implies the damping factor d does not have any effect on the saddle-node bifurcation where the determinant of the linearized Jocobian matrix must be zero. Hence the saddle-node bifurcation is a vertical wall in the d direction in the parameter space. For Hopf bifurcation and torus bifurcation, both P_m and d do play important roles in the bifurcation computation. The bifurcation loci can be computed numerically and the results are shown in Fig. 13 for variation in P_m and d. The curve 1, 2 and 4 are the loci of three Hopf bifurcations, and curve 5 is the torus bifurcation locus and the bifurcation points HB^1, HB^2, SNB^3, HB^4, and TR^{5-8} in Section 4 are on the curves 1–5 in Fig. 13, respectively.

We observe from Fig. 13 that the bifurcation loci for Eq. (14) divide the parameter space into six regions: (i) the left region of the curve 4 is the operating region of the system where the operating point (x_s) is locally stable; (ii) the region between curve 1 and 4 and above curve 5 where

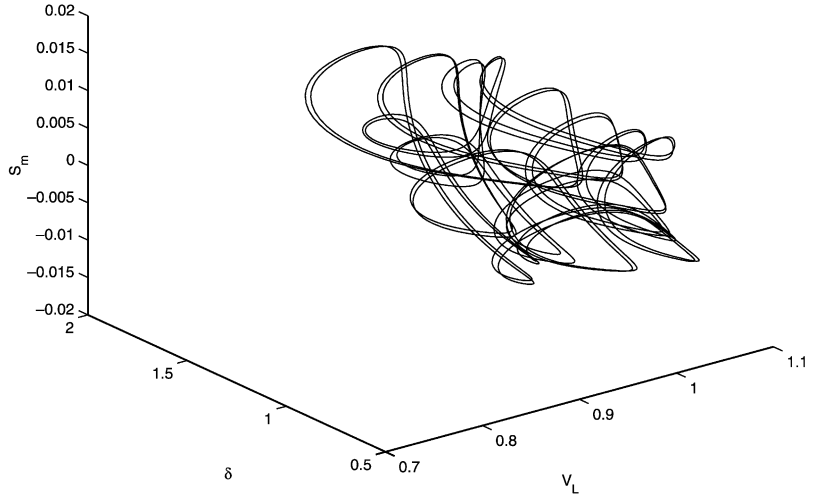

Fig. 8. The projection of the period-doubled trajectory for $P_m = 1.1288$.

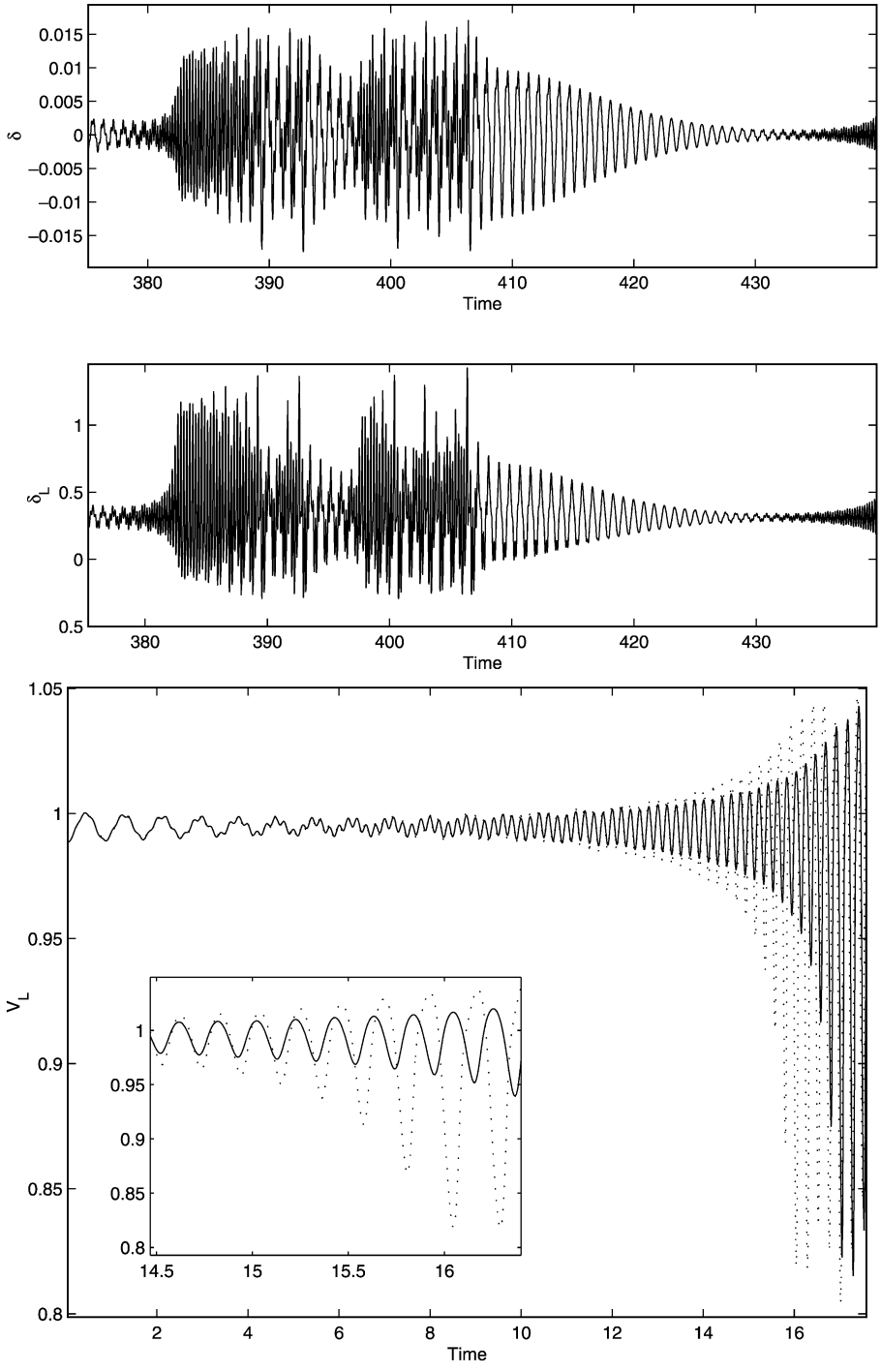

Fig. 9. The time simulations of the components E_{fdr}, V_L, δ and δ_L for $P_m = 1.135$, and the sensitive dependence of V_L on the initial conditions.

the equilibrium point x_s is locally unstable and a stable periodic solution exists (Fig. 4); (iii) the region surrounded by curve 1–3 where x_s is locally stable; (iv) the region surrounded by curve 2, 3 and P_m-axis, in which x_s is unstable; (v) the right region of curve 3 in which there is no equilibrium points, and (vi) the region surrounded by curve 5 and P_m-axis, where the dynamic behavior is the most complex one, there exist a quasi-periodic solution, chaos, phase-locked phenomena period-doubled orbits (see Section 4).

We will show that d can prevent the occurrence of torus bifurcation and stabilize the system. If we take a horizontal cross-section of the parameter plane in Fig. 13 by varying P_m while keeping d at a constant values, the cross-section will have four intersections with curve 5 for small d. In other

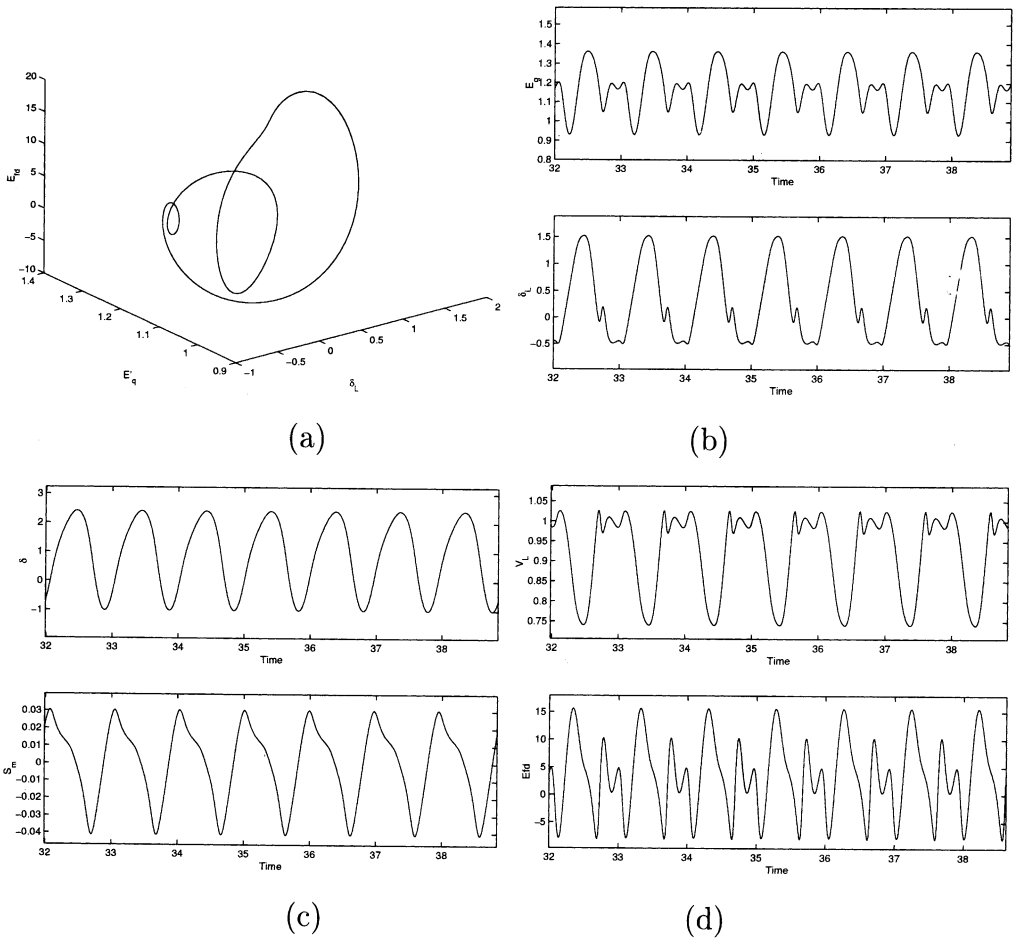

Fig. 10. The numerical simulations for $P_m = 0.9554$: (a), the projection of period-one orbit, (b)–(d), the corresponding sample time behavior of all system components.

words, four torus bifurcations will occur just like the case of $d = 0.05$ in Section 4. While the cross-section moves upward slowly, the number of the intersections decreases, and at last there is no intersection when d is greater than the largest value of d on curve 5 (approximately equal to 8.043). Therefore, torus bifurcations can be inhibited by d so that it can prevent complex phenomena resulted from torus bifurcation, and enhance the stability of the power system. In order to illustrate the inhibition, we present the projections of trajectories in Fig. 14 for $d = 10$. Parameters of the trajectories in the figures are the same as those in Fig. 5 except $d = 0.05$. By numerical simulations (we got the results, but deleted these because the file is too large), we observe that the quasi-periodic orbit in Fig. 5, the chaos and the diverging trajectories all become the periodic solutions in Fig. 14 when d changes from 0.05 to 10. Hence, the increasing in d contributes to the stability of the system.

Besides, note the stable region of x_s will increase when the cross-section goes up, i.e. the increase in the damping factor d contributes to the stable region for x_s or the feasibility region of the system.

In the simulation of this paper, the damping d is set from $d = 0$ to 200. According to Ref. [7], the d typically ranges from $d = -10$ to 20 p.u. and the values above $d = 100$ are mainly of academic interest. Here we just want to display the locus of bifurcation points completely. For the curve 2 of Fig. 13, i.e. the locus of HB^2, meets with the saddle-node bifurcation locus (curve 3) at last. Therefore, increases in d can deter the emergence of HB^2 to the saddle-node bifurcation. This result is similar to that about machine damping in the four-order model of power systems, in which machine damping can inhibit the emergence of Hopf bifurcation so that it can prevent the chaos resulted from period-doubling bifurcations [19]. However, the effect of the damping factor d is not as significant as that of the machine damping.

6. The role of hard-limits in the system

This section investigates the role of hard-limits in stability and bifurcation of the system. First assume that

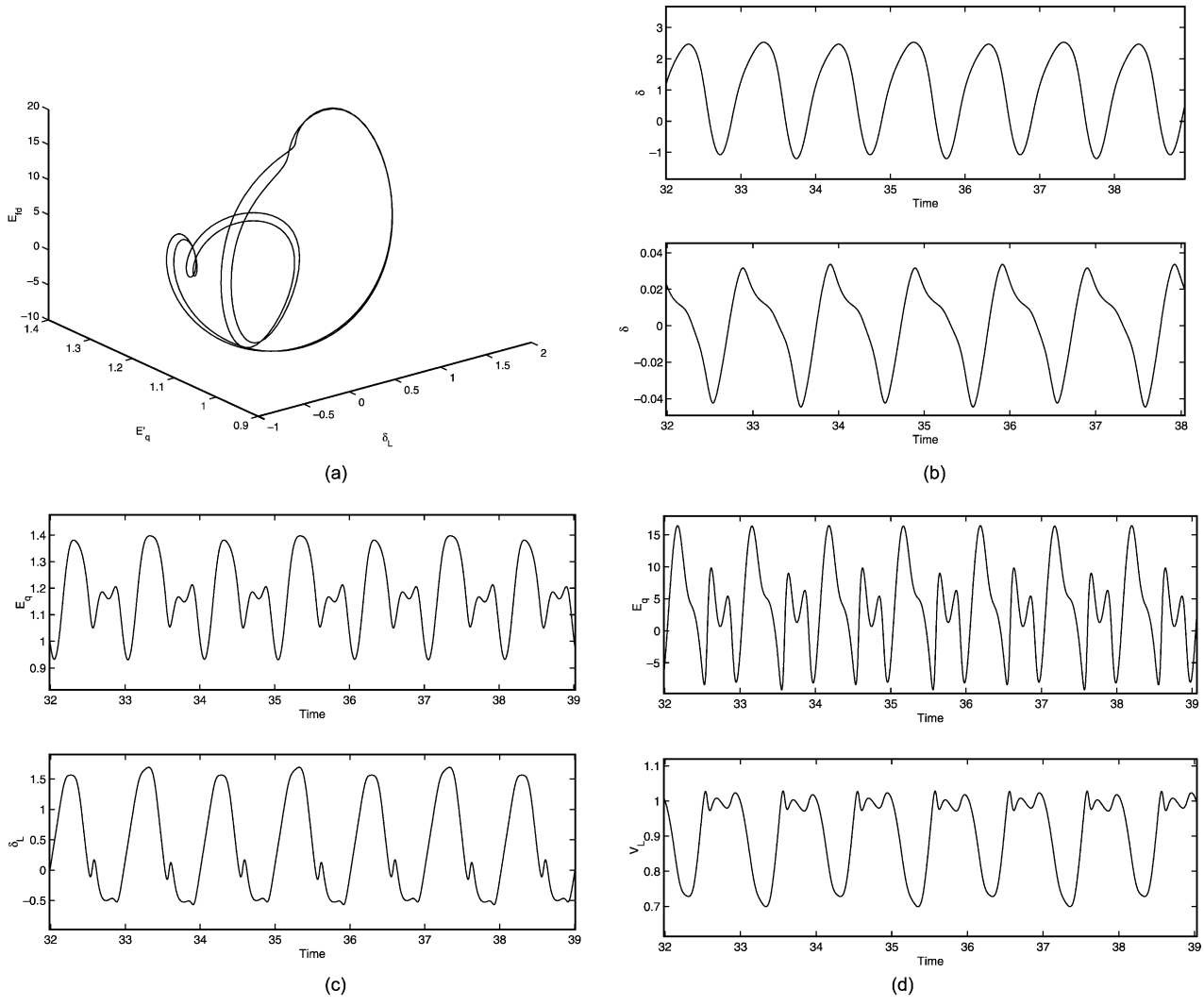

Fig. 11. The numerical simulations for $P_{\mathrm{m}} = 0.961$: (a), the projection of period-two orbit and (b)–(d), the corresponding sample time behavior of all system components.

there is an excitation field control in the generator which is simply represented by the single-time-constant transfer function shown in Fig. 15. Note that the wind-up type hard-limit on the signal E_{fdr} limits the control output E_{fd} strictly between the values $E_{fd_{\min}}$ and $E_{fd_{\max}}$. With the assumptions, instead of Eq. (7), the equation for $\dot{E}_{fd}$ in system (14) is replaced by

$$\dot{E}_{fdr} = \frac{E_{fd0} - E_{fdr} + K_{\mathrm{A}}(V_{\mathrm{ref}} - V)}{T_{\mathrm{A}}},$$

and the system (14) becomes into a new system (14′), where E_{fd} is the output of the wind-up limiter or saturation:

$$E_{fd} = \begin{cases} E_{fd_{\max}} & \text{if } E_{fdr} > E_{fd_{\max}}, \\ E_{fdr} & \text{if } E_{fd_{\min}} \le E_{fdr} \le E_{fd_{\max}}, \\ E_{fd_{\min}} & \text{if } E_{fdr} < E_{fd_{\min}}. \end{cases} \tag{14′}$$

In system (14), P_{m} is a bifurcation parameter, and all other parameters are chosen to be the same as in Section 2 except: $E_{fd_{\min}} = 0$, $E_{fd_{\max}} = 5$. Before we start to solve for the equilibrium points and bifurcation points of the system (14′), we also assume that the field control output E_{fd} at the operating point must lie within the linear region of the hard-limit for small P_{m}, i.e. between $E_{fd_{\min}}$ and $E_{fd_{\max}}$. In fact, the steady-state value of E_{fdr} should always lie within these limiting values in a well-designed system even under load variations. By using AUTO97, the bifurcation diagram for fixed $d = 0.05$ is drawn in Fig. 16, and P_{m} values of all bifurcation points are listed as the following: HB[1] for $P_{\mathrm{m}}^1 = 1.15586$; HB[2] for $P_{\mathrm{m}}^2 = 1.1913$; SNB[3] for $P_{\mathrm{m}}^3 = 1.9365$; HB[4] for $P_{\mathrm{m}}^4 = 0.60866$; CFB[5] for $P_{\mathrm{m}}^5 = 1.164358$.

From Fig. 16, it can be observed that the stable periodic solution jumping from the supercritical Hopf

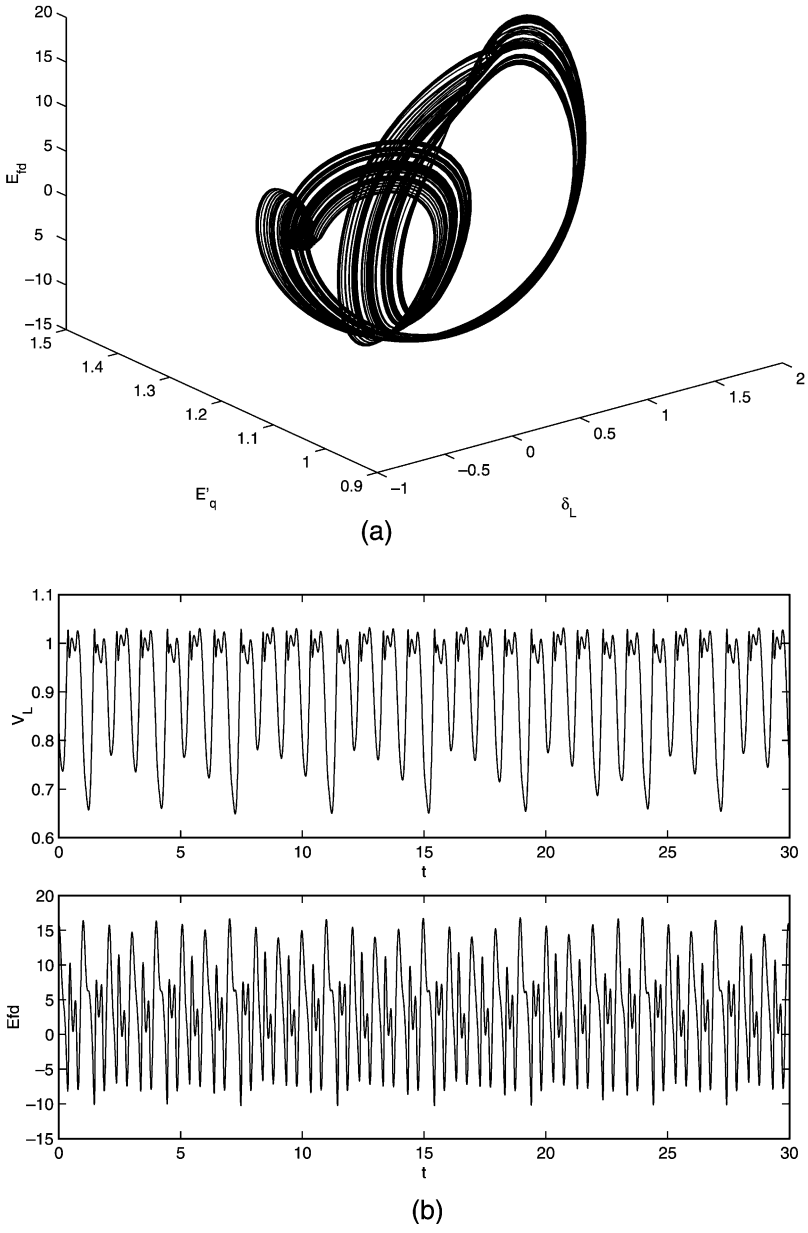

Fig. 12. The numerical simulations for $P_m = 0.965$: (a), the projection of the chaotic trajectory and (b) the corresponding sample time behaviors of V_L and E_{fd}.

bifurcation point HB[4] only undergoes a cyclic fold bifurcation at CFB[5], and then arrives at HB[1], a subcritical Hopf bifurcation. This means that the hard-limits inhibit torus bifurcations, which do occur for the case without hard-limits (Fig. 2). Therefore, a series complex dynamic behaviors resulted from torus bifurcations are all prevented. Moreover, it seems that the role of the hard-limits is more effective than the role of damping factor d in the sense of inhibiting torus bifurcation. To clarify this point we examine several time-plots of three trajectories when the hard-limits are introduced and find the system in the sustained oscillations and the quasi-periodic trajectory, chaos, and the diverging trajectory will converge to a stable limit cycle due to hard-limits. In other words, the hard-limits somehow introduce positive damping in a global sense so that torus bifurcations are prevented and the trajectories are eventually stabilized into sustained oscillation.

HB[2] is a subcritical bifurcation, where a branch of unstable periodic solutions emerge from it, but the branch is always unstable although it also undergoes a cyclic fold bifurcation CFB[6]. From Figs. 2 and 16, clearly the period-doubling bifurcation point in Fig. 2 are inhibited by the hard-limits so that the chaos resulted from period-doubling bifurcation is also prevented by the hard-limits. The numerical results further confirm that the hard-limits contribute to the stability of the system. When $P_m > P_m^2$, the transients diverge away quickly.

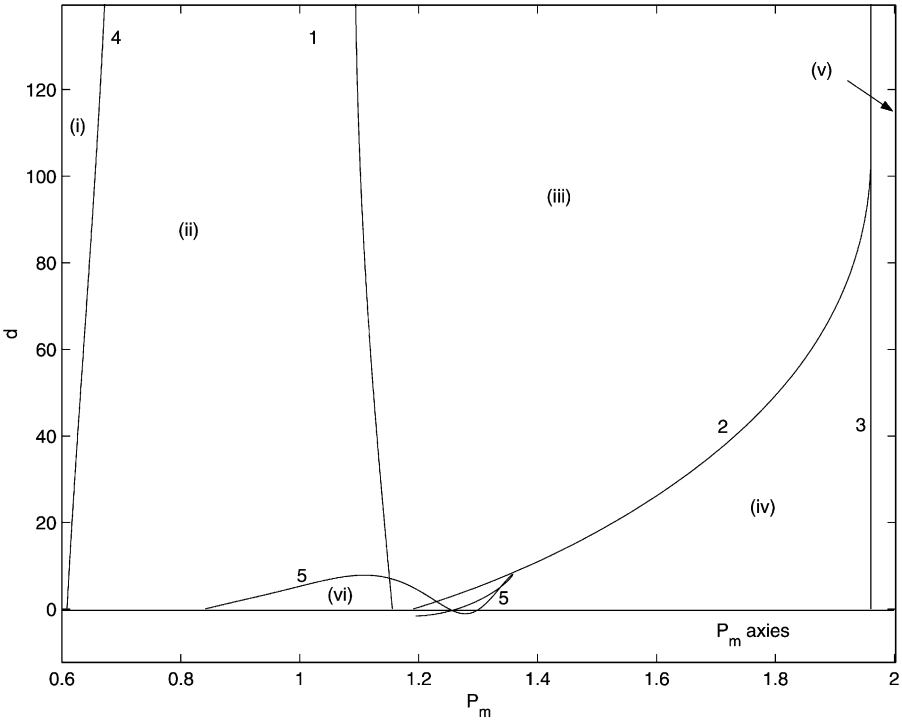

Fig. 13. The locus of bifurcation points in the parameter space $P_m - d$.

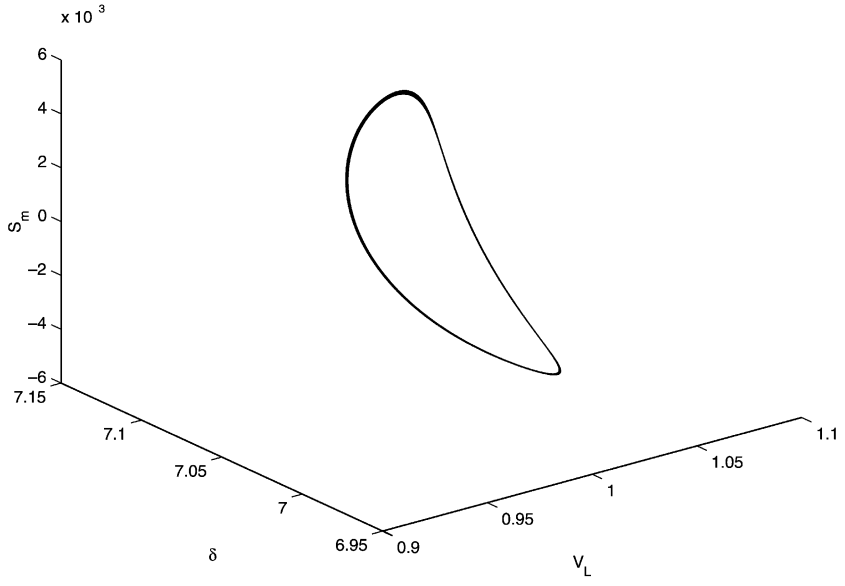

Fig. 14. The projection of the trajectory with the same parameters in Fig. 5 for $P_m = 0.851$, but $d = 10$.

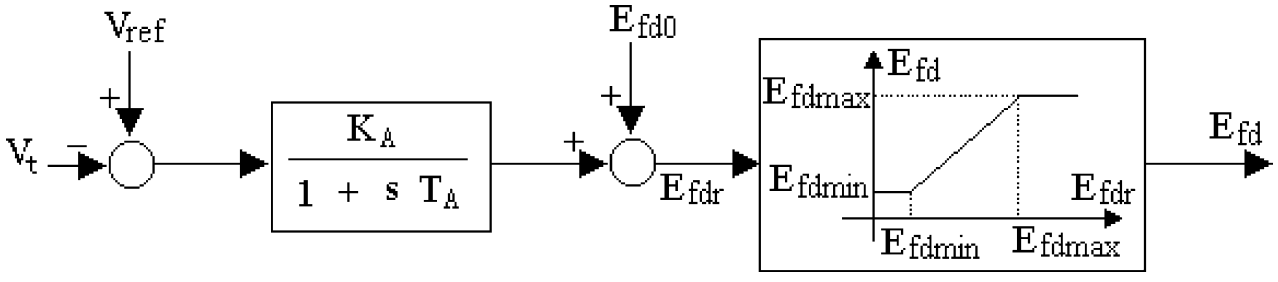

Fig. 15. The simplified excitation model.

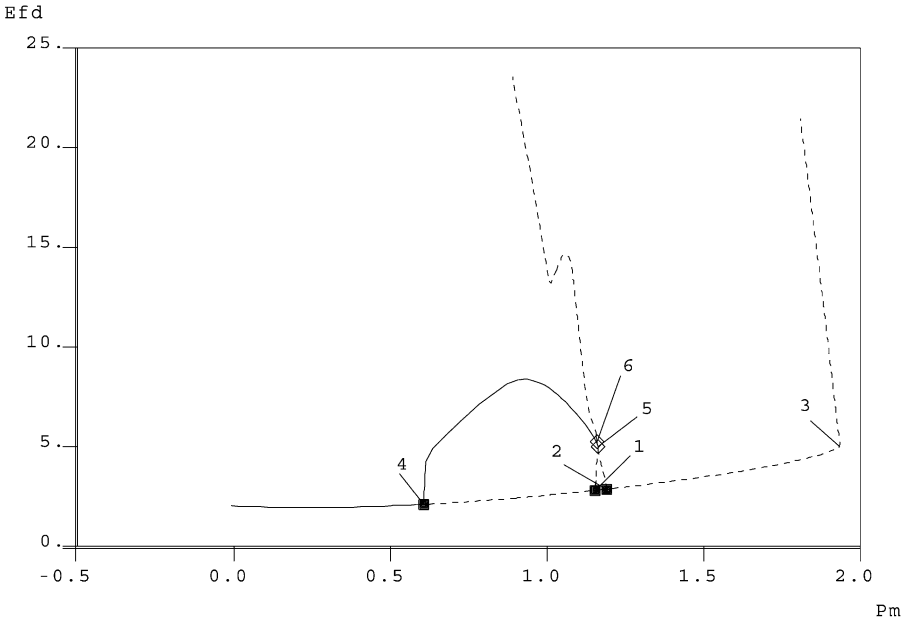

Fig. 16. The bifurcation diagram for the system with hard-limits for $d = 0.05$.

The preceding paragraph discusses the role of hard-limits while the damping factor $d = 0.05$. A natural question is whether or not this role exists persistently robustly. We carry out the same work but substituting $d = 10$ for $d = 0.05$. The result is shown in Fig. 17. Surprising similarities exist between Figs. 16 and 17, which demonstrate the role of hard-limits is identical for different d values.

Besides, note that the points CFB^5 in Figs. 16 and 17 are between HB^1 and HB^2, and the operating point for small P_m can move along the branch of stable periodic orbits, and then arrive at another feasibility region for larger P_m. Therefore, the two operating regions are connected by the branch of periodic solutions. The cyclic fold bifurcation is contributed to the hard-limits, where E_{fdr} arrives at $E_{fd_{max}}$.

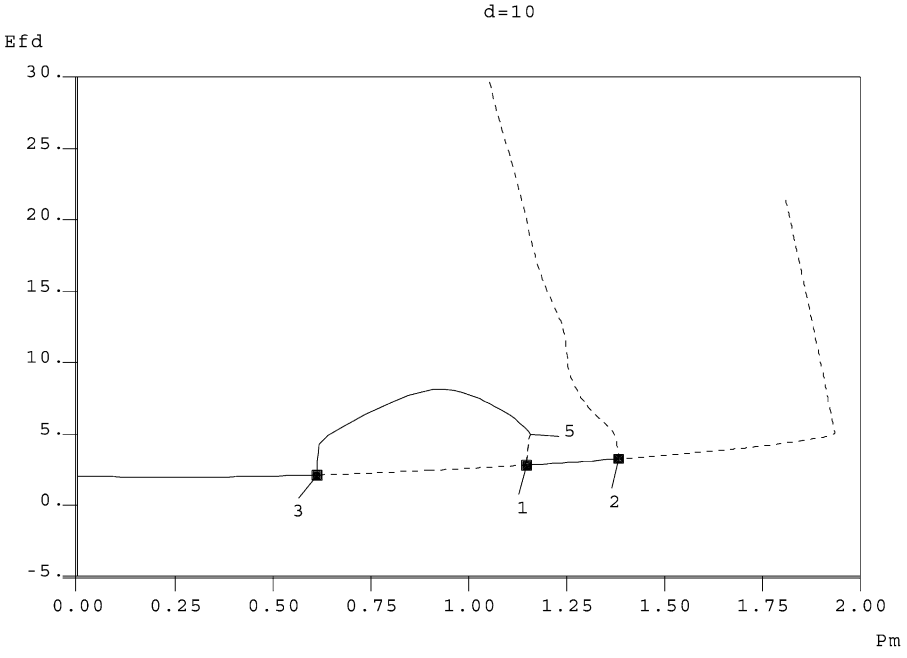

Fig. 17. The bifurcation diagram for the system with hard-limits for $d = 10$.

7. Conclusion

We found many dynamical bifurcations, emerging from the Hopf bifurcations in the model (14), including cyclic fold bifurcation, period-doubling bifurcations and torus bifurcations which all occur prior to the saddle-node bifurcation. We also observed the complex dynamical behaviors emerging from the dynamical bifurcations including periodic orbits, quasi-periodic orbits, phase-locking phenomena and two different routes to chaos and the intermittency mechanism of chaos. The stable periodic orbit emerges from HB^4 at $P_m^4 = 0.608664$. The three chaotic regions are also numerically observed: the chaos resulted from period-doubling bifurcations approximately lies in the interval $P_m \in [0.963, 0.965]$ and $P_m \in [1.1292, 1.135]$, and we only give the chaotic attractor is shown in Fig. 12; another chaotic attractor resulted from the quasi-periodic orbits approximately lies in the region $P_m \in [1.09706, 1.122]$, and the phase-locked phenomena approximately occurs in the region $P_m \in [1.0454, 1.09]$, and the corresponding chaotic attractors are obtained, but we deleted these. The above complex dynamical phenomena emphasize the importance of the consideration of nonlinearity.

In general, static bifurcations (saddle-node bifurcations) can be related to system collapse, and the oscillations of the quasi-periodic orbits or weak chaos affect the quality of electric power by distorting the voltage and current wave forms and can also cause the power system collapse in certain circumstances. But they are considered as one of the clues for the collapse of complicated power systems or for stability margin narrowing in parameter space.

Besides, we also find that at different Hopf bifurcation points, the system behavior is dominated by different state variables for instance δ and S_m at HB^1 and HB^4, and δ_L and V_L at HB^2. This fact suggests that different factors of power systems reduce the system stability at different critical points. In other words, we should design different control systems or control different parameters near the critical points.

When the effects of the damping factor d on the system's dynamics are considered, the torus bifurcation can be inhibited by the increases in d, which implies positive damping is beneficial for the stability of the system. Once the hard-limits are introduced to the system, the effects are similar to those of a great increase in the damping factor, i.e. the torus bifurcation is prevented. In Section 5, we do not investigate the loci of the cyclic bifurcation and period-doubling bifurcation like CFB^9, PDB^{10} for variations in both P_m and d. However, from the analyses of Sections 4 and 5, we can reasonably infer that the damping factor d also exists the largest values along the loci of the cyclic bifurcation and period-doubling bifurcation (they may be smaller than the largest value along the torus bifurcation locus). Therefore d also prevents the cyclic bifurcation and period-doubling bifurcation.

Remark. The size of the original file is too large ($> 33M$), present file near $2M$ after deleted a lot of Figures, for examples: the projections of quasi-periodic trajectory and chaotic trajectories and corresponding time behaviors of V_L for $P_m = 0.901$, 1.043, 1.09706, 1.105, 1.117, 1.122; the projections and time simulations of components of E_{fdr} and V_L of period-four, period-eight, chaotic behaviors for $P_m = 0.9623$, 0.9627, 1.12923, 1.1295, 1.135, 1.145; the time-plots of the trajectories with hard-limits for $P_m = 0.851$, 1.12923, 1.145.

Acknowledgements

This work is supported by the National Key Basic Research Fund (No. G1998020307) and the National Natural Science Foundation.

References

[1] Abed EH, Varaiya PP. Nonlinear oscillations in power systems. Int J Electr Power Energy Syst 1984;(6):37–43.
[2] Abed EH, Wang HD, Alexander JC, Hamdan AMA, Lee HC. Dynamic bifurcations in a power system model exhibiting voltage collapse. Int J Bifurcation Chaos 1993;3(5):1169–76.
[3] Ajjarapu V, Lee B. Bifurcation theory and its application to nonlinear dynamical phenomena in an electrical power system. Trans Power Syst 1992;l7(1):424–31.
[4] Dobson I, Chiang HD. Towards a theory of voltage collapse in electric power systems. Syst Control Lett 1989;13:253–62.
[5] Doedel EJ, Fairgrieve FT, Wang X. AUTO97 continuation and bifurcation software for ordinary differential equation; 1997.
[6] Guckenheimer J, Holmes P. Nonlinear oscillations, dynamical systems and bifurcations of vector fields, 2nd ed. New York: Springer; 1986.
[7] Ji W, Venkatasubramanian V. Hard-limit induced chaos in a fundamental power system model. Electr Power Energy Syst 1996; 18(5):279–95.
[8] Kundur P. Power system stability and control. The EPR power system engineering series, New York: McGraw-Hill; 1994.
[9] Kwatny HG, Pasrija AK, Bahar LY. Static bifurcation in electric power networks: loss of steady-state stability and voltage collapse. IEEE Trans Circ Syst 1986;33:981–91.
[10] Lee B, Ajjarapu V. Period-doubling route to chaos in an electrical power system. IEEE Proc C 1993;140(6):490–6.
[11] Modelling of voltage collapse including dynamic phenomena. Final Report. CIGRE Task Force 38-02-10; December 1992.
[12] Nayfeh AH, Balachandran B. Applied nonlinear dynamics analytical computational, and experimental methods; 1995.
[13] Nayfeh AH, Ahmad M, Char MC. Bifurcations in a power system model. Int J Bifurcation Chaos 1996;6(3):497–512.
[14] Padiyar KR. Power system dynamics-stability and control. Singapore: Wiley; 1996.
[15] Parker TS, Chua LO. Practical numerical algorithms for chaotic systems. New York: Springer; 1989.
[16] Rajesh GK, Padiyar KR. Analysis of bifurcations in a power system model with excitation limits. Int J Bifurcation Chaos 2001;11(9): 2509–16.
[17] Rajesh KG, Padiyar KR. Bifurcation analysis of a three node power system with detailed models. Electr Power Energy Syst 1999;21: 375–93.

[18] Shen JQ, Jing ZJ. A new detecting method for conditions of existence of Hopf bifurcation. ACTA Math Appl Sinica 1995; 11(1):79–93.
[19] Tan CW, Varghese M, Varaiya P, Wu FF. Bifurcation, chaos, and voltage collapse in power systems. Proc IEEE 1995;83(11): 1484–96.
[20] Venkatasubramanian V, Jiang X, Schattler H, Zaborszky J. Current status of the taxonomy theory DAE systems with hard-limits. Proceedings of the NSF International Workshop on Bulk Power System Voltage Phenomena—III, Davos, Switzerland; 1994. p. 15–103.
[21] Walve K. Modelling of power system components at severe disturbances. CIGRE paper 38-18. International Conference on Large High Voltage Electric Systems; August 1986.
[22] Wiggins S. Introduction to applied nonlinear dynamical systems and chaos. Texts in applied mathematics, vol. 2. Berlin: Springer; 1990.